Protein Structure and Folding:

Crystal Structure of the *Bacillus subtilis* Phosphodiesterase PhoD Reveals an Iron and Calcium-containing Active Site

Fernanda Rodriguez, James Lillington, Steven Johnson, Christiane R. Timmel, Susan M. Lea and Ben C. Berks

J. Biol. Chem. 2014, 289:30889-30899.
doi: 10.1074/jbc.M114.604892 originally published online September 12, 2014

⌘ *Author's Choice*

THE JOURNAL OF BIOLOGICAL CHEMISTRY VOL. 289, NO. 45, pp. 30889–30899, November 7, 2014

Crystal Structure of the *Bacillus subtilis* Phosphodiesterase PhoD Reveals an Iron and Calcium-containing Active Site◆

Received for publication, August 15, 2014, and in revised form, September 9, 2014 Published, JBC Papers in Press, September 12, 2014, DOI 10.1074/jbc.M114.604892

Fernanda Rodriguez[‡1,2], James Lillington[§¶1,3], Steven Johnson[§4], Christiane R. Timmel[¶], Susan M. Lea[§5], and Ben C. Berks[‡6]

From the [‡]Department of Biochemistry, University of Oxford, South Parks Road, Oxford OX1 3QU, the [§]Sir William Dunn School of Pathology, University of Oxford, South Parks Road, Oxford OX1 3RE, and the [¶]Inorganic Chemistry Laboratory, University of Oxford, South Parks Road, Oxford OX1 3QR, United Kingdom.

Background: PhoD family enzymes liberate phosphate from organic compounds.
Results: The structure of PhoD reveals an active site with one Fe^{3+} and two Ca^{2+} ions.
Conclusion: PhoD represents a new class of phosphatase related to purple acid phosphatases.
Significance: The requirement of PhoD for iron ions may limit bacterial phosphate acquisition in low iron environments.

The PhoD family of extra-cytoplasmic phosphodiesterases are among the most commonly occurring bacterial phosphatases. The exemplars for this family are the PhoD protein of *Bacillus subtilis* and the phospholipase D of *Streptomyces chromofuscus*. We present the crystal structure of *B. subtilis* PhoD. PhoD is most closely related to purple acid phosphatases (PAPs) with both types of enzyme containing a tyrosinate-ligated Fe^{3+} ion. However, the PhoD active site diverges from that found in PAPs and uses two Ca^{2+} ions instead of the single extra Fe^{2+}, Mn^{2+}, or Zn^{2+} ion present in PAPs. The PhoD crystals contain a phosphate molecule that coordinates all three active site metal ions and that is proposed to represent a product complex. A C-terminal helix lies over the active site and controls access to the catalytic center. The structure of PhoD defines a new phosphatase active site architecture based on Fe^{3+} and Ca^{2+} ions.

Under conditions of phosphate deficiency bacteria attempt to mobilize phosphate from organic molecules by synthesizing extra-cytoplasmic alkaline phosphatase enzymes. Analysis of the Global Ocean Survey metagenomic data set (1) suggests that these extra-cytoplasmic alkaline phosphatases come predominantly from the PhoA, PhoX, and PhoD families, with genes encoding PhoD enzymes being as abundant as those of the other two enzyme families combined (2).

PhoA family enzymes are predominantly phosphomonoesterases. The active site of the prototypical PhoA enzyme of *Escherichia coli* contains two Zn^{2+} and one Mg^{2+} ion, and the catalytic mechanism involves an enzyme-bound phosphoserine intermediate (3). PhoX enzymes are exclusively phosphomonoesterases, and their complex active site cofactor has recently been shown to contain two Fe^{3+} ions, three Ca^{2+} ions, and a μ_3-bridging oxo group (4).

Enzymes of the PhoD family are the least well characterized of the three major classes of bacterial extra-cytoplasmic alkaline phosphatase. The archetype of the family is *Bacillus subtilis* PhoD. This enzyme is a phosphodiesterase but also has significant phosphomonoesterase activity (5). Metal ion reconstitution experiments show that PhoD requires Ca^{2+} for activity (5). The physiological role of PhoD is proposed to be the release of phosphate from cell wall teichoic acids under conditions of phosphate starvation (6). A second biochemically characterized member of the PhoD family is the secreted phospholipase D (PLD)[7] from *Streptomyces chromofuscus* (7). PLD cleaves the phosphodiester bond that links the head group and diacyl glycerol portions of phospholipids. PLD is reported to contain one iron atom together with substoichiometric amounts of manganese. In addition, the enzyme requires Ca^{2+} ions for significant activity and to bind to phospholipid membranes.

Sequence analysis suggests that PhoD proteins are unrelated to the PhoA or PhoX phosphatase families but instead form a distinct subgroup within a very broad structural superfamily of hydrolytic enzymes possessing binuclear metal centers at the active site (the "metallophosphatase" superfamily in the Conserved Domain Database (8)). Within this structural superfamily it has been argued that the PhoD family has greatest similarity to eukaryotic purple acid phosphatases (PAPs) (9). In PAPs the active site metal pair are a Fe^{3+} ion and a divalent ion that can be Fe^{2+}, Mn^{2+}, or Zn^{2+} depending on the enzyme (10, 11). The Fe^{3+} ion is ligated by a tyrosine ligand resulting in an intense phenolate-to-Fe(III) charge-transfer transition (λ_{max} =

◆ This article was selected as a Paper of the Week.
⌘ *Author's Choice*—Final version full access.
The atomic coordinates and structure factors (code 2YEQ) have been deposited in the Protein Data Bank (http://wwpdb.org/).

[1] Both authors contributed equally to this work.
[2] Supported by an European Molecular Biology Organization (EMBO) Fellowship and by the E. P. Abrahams Cephalosporin Trust Fund. Present address: Instituto de Procesos Biotecnologicos y Quimicos (IPROBYQ-CONICET, UNR), Suipacha 531, 2000 Rosario, Argentina.
[3] Recipient of a studentship from the Engineering and Physical Sciences Research Council and also received funding from the Oxford Martin School Vaccine Design Institute (of which S. M. L. is Co-director). Present address: Birkbeck College, Malet St., London WC1E 7HX, United Kingdom.
[4] Funded by Medical Research Council (MRC) Programme Grant G0900888 (to S. M. L.).
[5] To whom correspondence may be addressed. Tel.: 44-1865-275181; Fax: 44-1865-275515; E-mail: susan.lea@path.ox.ac.uk.
[6] To whom correspondence may be addressed. Tel.: 44-1865-613294, Fax: 44-1865-613201; E-mail: ben.berks@bioch.ox.ac.uk.

[7] The abbreviations used are: PLD, phospholipase D; PAP, purple acid phosphatase; pNPP, *p*-nitrophenyl phosphate; bis-pNPP, bis-*p*-nitrophenyl phosphate.

510–560 nm; $\epsilon = \sim 3000-4000\ \text{M}^{-1}\ \text{cm}^{-1}$), which gives PAPs their characteristic purple color. The occurrence of a tyrosinate-ligated Fe^{3+} ion is highly characteristic for PAPs, with the only other currently identified examples being found in the structurally unrelated diferric DNA ligase from *Ferroplasma acidiphilum* (12). It is, thus, striking that *S. chromofuscus* PLD exhibits a PAPS-like visible spectrum. Amino acid residues, including a tyrosine, that could correspond to the Fe^{3+} ligands in PLD have been proposed on the basis of sequence conservation and mutagenesis experiments (9).

In an effort to define the active site architecture of the PhoD phosphatase family we have determined the structure of *B. subtilis* PhoD. Unexpectedly, the active site contains three metal ions, these being identified as a Fe^{3+} ion and two Ca^{2+} ions. Our structural data show that the PhoD active site is distinct from that found in PAPs but that these two enzyme families conserve the position and coordination environment of their Fe^{3+} ions. A phosphate molecule bound to the PhoD active site gives insight into the mechanism of catalysis.

EXPERIMENTAL PROCEDURES

Cloning—The sequence coding for the mature domain of PhoD (codons 57–593) was amplified from *B. subtilis* strain 168 chromosomal DNA using the primers 5′-CCAGTGGGTCTC-AGGTGGTGCGCCTAACTAAGC-3′ and 5′-CGGCGTCG-ACTTAATTCGTGATTTTTGCACG-3′. The resulting amplicon was digested with BsaI and SalI and cloned into the same sites in plasmid pCA597 (13) to produce plasmid pCA597-*mphoD*. This plasmid directs the expression of the mature domain of PhoD with a Ulp1-cleavable N-terminal Strep-SUMO tag (where SUMO is small ubiquitin-like modifier). Site-specific mutations were introduced into the *phoD* coding sequence in plasmid pCA597-*mphoD* using the QuikChange™ method (Stratagene).

Protein Purification—E. coli strain BL21 (DE3)(14) containing plasmids pCA597-*mphoD* and pRARE (Novagen) was grown aerobically at 37 °C in 2×YT medium (Sigma-Aldrich) supplemented with 50 μg/ml kanamycin. Protein expression was induced at an $A_{600\ \text{nm}} = 0.6$ with 0.5 mM isopropyl-1-thio-β-D-galactopyranoside, and the culture grown was then grown for 15 h at 20 °C.

Cells were harvested by centrifugation and resuspended in resuspension buffer (20 mM Hepes NaOH, pH 7.4, 200 mM NaCl, 1 mM $CaCl_2$), with EDTA-free complete protease inhibitors (Roche Applied Science) and DNase I (Sigma-Aldrich). The cells were broken by three passages through a French press at 8000 p.s.i. The lysate was clarified by successive centrifugation at 10,000 × *g* for 20 min at 4 °C and at 45,000 × *g* for 1 h at 4 °C, and then applied to a 5-ml self-packaged Strep-Tactin column (IBA, GmbH, Göttingen, Germany). Recombinant PhoD was eluted from the column with resuspension buffer containing 2.5 mM desthiobiotin and then supplemented with 1 mg of His_6-Ulp1 protease (13) and dialyzed overnight at 4 °C against resuspension buffer. Cleaved tags and uncleaved mPhoD protein were removed by incubation with Strep-Tactin matrix, and the sample was further purified on a Superdex75 (16/60) prep grade size-exclusion column (GE Healthcare) that had been equilibrated in resuspension buffer. The mPhoD-containing fractions were pooled and concentrated using a 30-kDa cut-off Amicon PLTK Ultracel-PL membrane concentrator (Merck Millipore).

Phosphatase Activity Assays—Alkaline phosphatase activity was assayed spectrophotometrically by measuring the release of *p*-nitrophenol from *p*-nitrophenyl phosphate (pNPP) or bis-*p*-nitrophenyl phosphate (bis-pNPP). Assays were started by the addition of 1 μg/ml PhoD to 100 mM Tris-HCl, pH 8.0, 2 mM $CaCl_2$, and 1 mM pNPP or bis-pNPP at 25 °C. Reactions were stopped after 5 min by the addition of 1 M final concentration NaOH. *p*-Nitrophenol production was quantified using $\epsilon_{405\ \text{nm}} = 18{,}000\ \text{M}^{-1}\ \text{cm}^{-1}$.

The substrate specificity of PhoD was assessed by measuring phosphate release from test substrates. Each 800-μl reaction contained 100 mM Tris-HCl, pH 8.0, 2 mM $CaCl_2$, 1 mM test substrate, and 1 μg of PhoD. After a 5-min incubation at 25 °C the reaction was terminated by the addition of 200 μl of malachite green reagent (AMS Biotechnology) followed by incubation at room temperature for 30 min. Production of phosphate was obtained from absorbance at 620 nm and quantified using a phosphate standard curve.

Crystallographic Data Collection and Structure Determination—Crystallization trials were performed at 294 K by the sitting drop vapor diffusion method. The best crystals were obtained in 0.2 M NaCl, 0.1 M Na_2HPO4/KH_2PO4, 54% PEG 200, pH 5.6, with protein at 7.8 mg/ml, a total drop volume of 400 nl, and a 50:50 protein-to-mother liquor ratio. The crystals were cryo-protected in mother liquor containing 10% (w/v) ethylene glycol and flash-cooled in liquid nitrogen. X-ray data were collected at beamlines ID23_1 (European Synchrotron Radiation Facility (ESRF), Grenoble, France) and I03 (Diamond Light Source, Oxfordshire, UK). The data were processed in space group I4122 using Process (part of the autoPROC pipeline; Global Phasing Ltd.) (15). The multiple wavelength anomalous diffraction method was used to determine the sites of the three catalytic metals (initially assigned as three iron sites, but later refined as one iron and two calcium sites) using autoSharp (16) and to produce phases that were optimally solvent-flattened to 62% using Solomon (17). The handedness of the sites was determined by the contrast (standard deviation of solvent to standard deviation of protein) falling from 57 to 27% in one hand and from 63 to 39% in the other. Buccaneer (18) built a partial model among a number of other unlikely chains. This model was then manually manipulated in accordance with the kidney bean purple acid phosphatase structure (Protein Data Bank (PDB) 3KBP). Input of this partial model for a second round of Buccaneer building placed 524 residues of a monomer into the map. This was used as the search model for molecular replacement via MOLREP (19), placing the two translational related non-crystallographic symmetry copies at (0.5, 0.5, 0.08) of the unit cell from one another. Iterative refinement and model building were carried out with Refmac (20) and Coot (21). The quality of the model was checked using MolProbity (22), with a final MolProbity score of 1.19 (93th percentile).

The sample for proton-induced x-ray emission (micro-PIXE) analysis was purified in a calcium-free buffer composed of 20 mM Tris-HCl, pH 7.2, 200 mM potassium acetate. Measurements were taken at the Ion Beam Centre (University of Surrey).

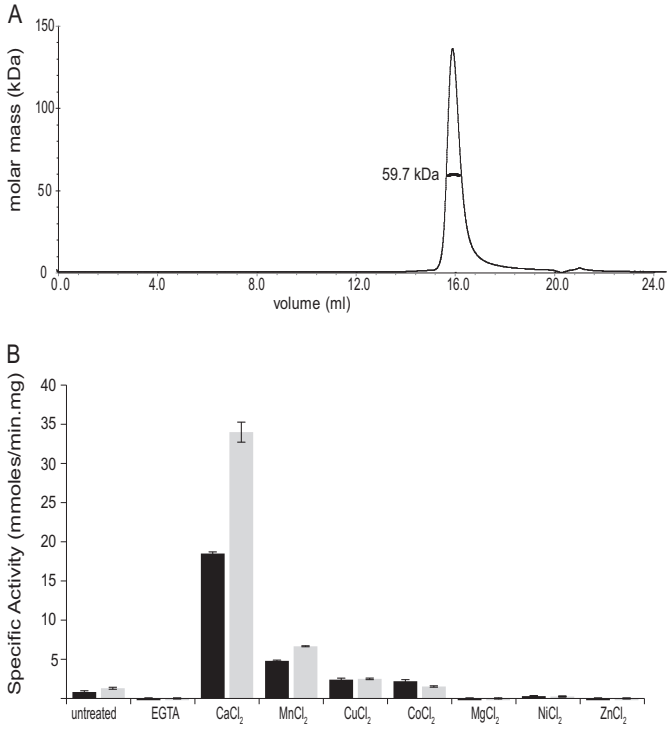

FIGURE 1. *A*, size-exclusion multi-angle laser light scattering analysis of PhoD. The buffer was 20 mM Hepes, pH 7.5, 400 mM NaCl, 2 mM calcium acetate, and the flow rate was 0.4 ml/min. A single species of weight-averaged molecular mass 59,700 Da (± 1%) is observed. *B*, phosphomonoesterase and phosphodiesterase activities of PhoD measured with pNPP (*black bars*) and bis-pNPP (*gray bars*), respectively. PhoD in 5 mM Tris-HCl, pH 8.0, was treated with 100 μM Na_2EGTA for 5 min (bar marked *EGTA*), and then 2 mM of the chloride salt of the indicated divalent metal cation was added. *Error bars* indicate the S.D. of three independent experiments.

EPR Spectroscopy—EPR spectra were collected on an X-band CW EPR spectrometer (Bruker Biospin GmbH) using an X-band Super High Sensitivity Probehead (Bruker) and equipped with a low temperature helium flow cryostat (Oxford Instruments CF935). Data were analyzed using the program EasySpin (23).

RESULTS

Characterization of B. subtilis PhoD—B. subtilis PhoD was heterologously expressed in the cytoplasm of *E. coli*. Purified recombinant PhoD protein was a monomer in solution as judged by size-exclusion multi-angle laser light scattering (Fig. 1*A*). The recombinant PhoD exhibited phosphomonoesterase activity with the colorigenic substrate pNPP and exhibited phosphodiesterase activity with the colorigenic substrate bis-pNPP (Fig. 1*B*). However, the specific activity of the recombinant enzyme was very much lower than previously reported for the native enzyme (5). We observed that the activity of the recombinant enzyme was massively enhanced by Ca^{2+} supplementation (Fig. 1*B*), and so Ca^{2+} was subsequently included in all buffers used for the purification and analysis of PhoD. At pH 8.0 and a temperature of 25 °C, the Ca^{2+}-supplemented recombinant PhoD protein had a K_m for pNPP of 50 μM and a k_{cat} of 1.2 s^{-1}. PhoD was able to release phosphate from compounds containing phosphoester bonds but was not able to cleave phosphorus-nitrogen or phosphorus-carbon bonds (Fig. 2*A*).

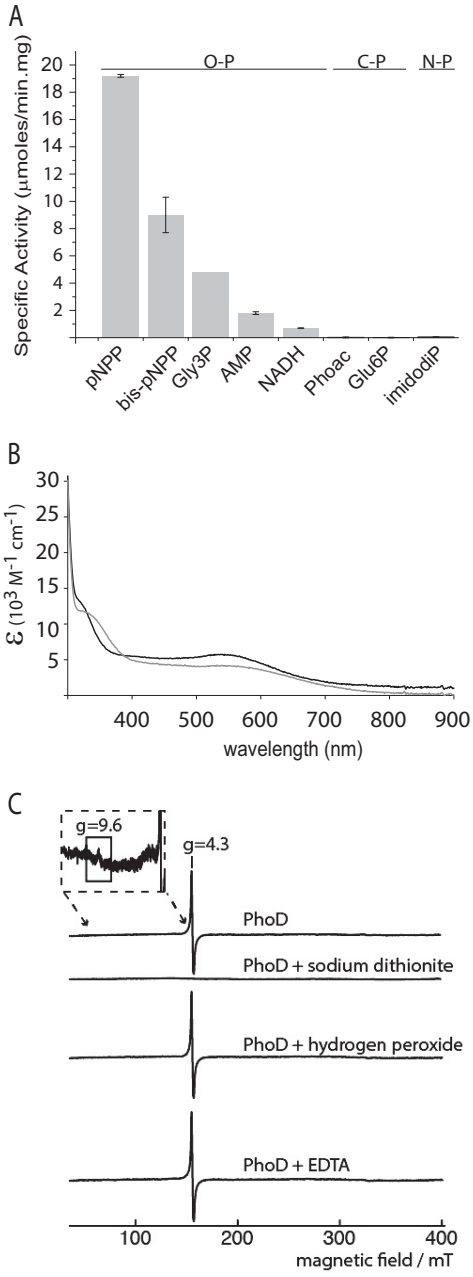

FIGURE 2. **Characterization of recombinant *B. subtilis* PhoD.** *A*, phosphate released from different substrates by PhoD. The assays contained 1 μg/ml PhoD and 1 mM of the test substrate in 100 mM Tris, pH 8.0, 2 mM $CaCl_2$. *Gly3P* is glycerol 3-phosphate; *Phoac* is phosphonoacetic acid; *Glu6P* is glucose 6-phosphate; *imidodiP* is imidodiphosphate. Substrates are grouped according to whether the target bond is between phosphorus and oxygen (O–P), phosphorus and carbon (C–P), or phosphorus and nitrogen (N–P). *Error bars* indicate the S.D. of three independent experiments. *B*, visible absorption spectrum of 2.3 mg/ml PhoD in 20 mM Hepes NaOH, pH 7.4, 200 mM NaCl, 1 mM $CaCl_2$ in the absence (*black*) or presence (gray) of 10 mM Na_2EGTA. *C*, EPR spectra of PhoD highlighting the g = 4.3 peak. Spectra are shown for native PhoD, PhoD with 5 mM sodium dithionite, PhoD with 2 mM hydrogen peroxide, and PhoD with 50 mM EDTA. The *inset* shows a magnified part of the spectrum around g = 9.6. The PhoD concentration was 10 mg/ml in 20 mM Hepes, pH 7.5, 400 mM NaCl, 2 mM calcium acetate with 20% (v/v) glycerol added. A control experiment showed that the glycerol added to the samples did not change the spectral line shape (data not shown). EPR operating conditions: microwave power, 2 milliwatts; microwave frequency, 9.425 GHz; modulation, 5.0 G at 100 kHz; temperature, 10 K. Spectra are buffer-subtracted, with negative controls taken for sodium dithionite, hydrogen peroxide, and EDTA solutions.

PhoD purified in the presence of Ca^{2+} was purple in color with a broad absorbance band in the visible spectrum, indicating the presence of a prosthetic group (Fig. 2*B*). The addition of the Ca^{2+}-selective chelator EGTA caused a shift in the visible absorbance maximum from around 540 nm to ~560 nm (Fig. 2*B*), suggesting that Ca^{2+} is associated with the prosthetic group. Proton-induced x-ray emission spectroscopy of PhoD purified in the absence of added Ca^{2+} ions detected iron and calcium but no cobalt, magnesium, manganese, nickel, or zinc. The presence of iron in PhoD was confirmed by EPR spectroscopy, which detected the g = 4.3 and weak g = 9.6 peaks characteristic of the middle and lower Kramer's doublets of an isolated high spin rhombic Fe^{3+} ion (Fig. 2*C*). No further signals were elicited by oxidation with hydrogen peroxide. All EPR signals disappeared on reduction with sodium dithionite, as expected of reduction of a monomeric Fe^{3+} ion to the EPR silent Fe^{2+} state (Fig. 2*C*). The Fe^{3+} signal was unperturbed by the addition of 50 mM EDTA (Fig. 2*C*), showing that the iron in PhoD is too tightly bound to be removed by chelator treatment. The presence of iron in PhoD has not previously been reported. However, iron is found in the homologous *S. chromofuscus* PLD enzyme (7).

Structure of PhoD—PhoD was crystallized at pH 5.6 in the presence of phosphate. The structure of PhoD was determined to a resolution of 2 Å via a multi-wavelength anomalous diffraction experiment using the iron cofactor as the source of the anomalous signal. Final R/R_{free} values at this resolution were 17.8/20.2%. Data reduction, phasing, and crystallographic refinement statistics are shown in Table 1. Every residue in the PhoD mature domain was observed in the electron density.

The core of the PhoD structure is a sandwich of two long β-sheets flanked by α-helices of varying lengths (Figs. 3*A* and 4). Three active site metal ions are coordinated by residues on loops on one face of the β-sandwich and are covered by a long C-terminal helix. With the knowledge that PhoD contains Fe^{3+} and Ca^{2+} ions (above) anomalous Fourier maps at three wavelengths allowed the assignment of the three active site metal ions as one Fe^{3+} ion and two Ca^{2+} ions, which we label Ca_A and Ca_B (Figs. 3, *B* and *C*, and 5*A*). Substitution of individual amino acids involved in metal ion coordination at each of the three metal sites either abolished (C180A, D265A, N271A, N272A, and D436A variants) or drastically reduced (D207A and D266A variants) PhoD activity with pNPP as a substrate (Fig. 5*B*), showing that all three metal ions are required for the phosphomonoesterase activity of PhoD.

PhoD was crystallized in the presence of phosphate, and the structure contains a phosphate molecule bound at the active site (Fig. 3*B*). Phosphate is a known competitive inhibitor of PhoD (5).

PhoD Has Structural Similarity to Purple Acid Phosphatases—A search of the PDB protein structure database using the DALI server (24) revealed that PhoD has highest structural similarity to PAPs. The closest overall structural match was to red kidney bean PAP (PDB 4DHL) (25) with a DALI *Z*-score of 28.6 and a main chain root mean square deviation relative to PhoD of 2.47 Å. The similarity between the two protein families is illustrated in Fig. 3, *A* and *B*, where we have chosen to compare PhoD with sweet potato PAP (PDB 1XZW) (26) due to the close structural homology in the way the two proteins bind phosphate (discussed below).

At the Fe^{3+} site the sole difference in amino acid ligand sets between PhoD and the PAPs is a cysteine-for-aspartate substitution in PhoD (Cys-180). Cysteine is an unusual ligand to a Fe^{3+} ion. Indeed, to the best of our knowledge, the structurally unrelated alkaline phosphatase PhoX (4) is the only other protein using a thiolate group to coordinate a redox-inactive Fe^{3+} ion. The visible absorbance bands of PhoD are likely to arise predominantly from the tyrosine ligation of the Fe^{3+} ion, as in the PAPs (27). However, additional thiolate-to-Fe^{3+} charge transfer bands from the cysteine ligand will also contribute to the visible spectrum (28).

The Ca_A site in PhoD corresponds to the position of the second metal site in the PAPs. Nevertheless, there is little similarity between the metal ion ligands found at this site in the two types of protein (Fig. 3*B*), consistent with the different coordination preferences of Ca^{2+} and the divalent metal ions found in the PAPs. Specifically, the Ca_A site has irregular 8-fold coordination with all amino acid ligation being provide by Asp residues.

The Ca_B site in PhoD has no analogue in the PAPs. The Ca_B ion has regular octahedral ligation with Asp and Asn ligands.

All three metal ions in PhoD have bonding interactions with the phosphate group present in the active site (Figs. 3*B* and 5*A*). One oxygen atom of the phosphate ligates the iron, one oxygen atom bridges Ca_A and the iron, and one oxygen atom bridges the two calcium ions. The interactions between the phosphate and the Ca_A-Fe pair replicate the tripodal μ–η2–η2-geometry observed between phosphate and the two metal ions of sweet potato PAP in PDB structure 1XZW (26)(Fig. 3*B*). A similar mode of bridging tripodal coordination has also been seen for phosphate bound to the dimetal centers of *Sporosarcina pasteurii* urease (29) and an organophosphate-degrading enzyme from *Agrobacterium radiobacter* (30). In addition to interacting with the active site metal ions the phosphate ion in PhoD has bonding interactions with the amino acid side chains of Arg-562 and His-566 from the C-terminal capping helix (Figs. 5*A* and 6, *A*–*C*).

The C-terminal Helix Occludes Access to the PhoD Active Site—The C-terminal region of the *B. subtilis* PhoD protein forms an α-helix (residues 560–577), which lies over the active site (Figs. 3*A* and 6). This helix is part of a C-terminal extension that is found in PhoD from *B. subtilis* and certain additional *Bacillus* species, but is absent from other bacterial PhoD proteins and from the PAPs (Fig. 6*A*). The C-terminal helix is held in position by a network of salt bridges, which include interactions with the phosphate ion located in the active site, and with Asp-436, which bridges the Fe and Ca_A ions (Fig. 6*C*).

The C-terminal helix blocks access to the catalytic site. Furthermore, as judged by modeling studies with pNPP substituted for the phosphate molecule seen in the crystal structure, steric clashes with the helix would also prevent substrates binding to the active site. As a consequence, the C-terminal helix must move from the position seen in the crystal structure in order for substrates to bind to PhoD. The main chain crystallographic B-factor for the C-terminal helix is high (49.1 $Å^2$) relative to the whole protein average (28.2 $Å^2$), showing that the C-terminal helix is more mobile than the rest of the PhoD structure (Fig. 6*D*). This suggests that the helix is relatively weakly bound to

TABLE 1
Data collection and refinement statistics

Data Collection	**ID23_1**			**IO3**
Space group	$I4_122$			
Molecules in asymmetric unit	2			
Unit cell parameters (Å,˚)	148.05, 148.05, 347.2, 90.0, 90.0, 90.0			
Solvent content (%)	38			
	Peak	Inflexion	Remote	
	(λ=1.73920Å)	(λ=1.74090Å)	(λ=1.73190Å)	(λ=1.28180Å)
Resolution range (Å)	173.6 – 2.7	174.7 – 3.7	174.2 – 3.2	135.6 -1.9 (2.0 – 1.9)
Number of Unique reflections	54642	20953	32169	141401 (19895)
Rmerge(%)	11(48)	16(49)	13(48)	7.5(49)
Rpim(%)	12(29)	18(25)	14(25)	5.3(38)
Mean I/σ(I)	15.6(4.0)	11.0(4.2)	14.1(4.4)	9.6(2.0)
Completeness (%)	100(100)	100(100)	100(100)	99(96)
Redundancy	8.4(6.8)	8.5(8.5)	8.5(8.4)	3.5(3.1)
MAD Phasing Statistics				
Sharp FOM (acentrics)	0.59 (136.19-11.94); 0.22(136.19 -2.75);0.11(2.82-2.68)			
Sharp FOM (centrics)	0.20 (136.19-11.94); 0.07(136.19 – 2.75);0.07(2.82-2.68)			
Sharp phasing power (iso/ano):	Peak (-)/0.487;Inflexion 0.086/0.328;Remote 0.023/0.250			
Acentric	Peak (-)/(-);Inflexion 0.082/(-);Remote 0.021/(-)			
Centric	Peak (-)/0.947;Inflexion 0.535/0.981;Remote 0.680/0.990			
Rcullis (acentrics)	Peak (-)/(-);Inflexion 0.490/(-);Remote 0.640/(-)			
	0.864			
Rcullis (centric)	0.2933/0.2681			
Solvent flattened FOM (overall)	0.6559/0.7956			
Solomon contrast start/end				
Sharp SigmaA				
Refinement summary:	`			
Resolution (Å)				136-1.9 (2.0 – 1.9)
R factor (%)				17.8 (29)
Free R factor (%)				20.2 (31)
R.m.s.d. bond lengths (Å)				0.014
R.ms.d. bond angles (˚)				1.3
No. atoms in asymmetric unit				20841
Of which: Protein				19772
Fe				2
Ca				4
Na				6
PEG200/EG				420 (73 units)
Phosphate				10 (2 units)
H20				627
Ramachandram plot:				
Preferred (%)				96
Allowed (%)				4
Outliers (%)				0
PDB code				2YEQ

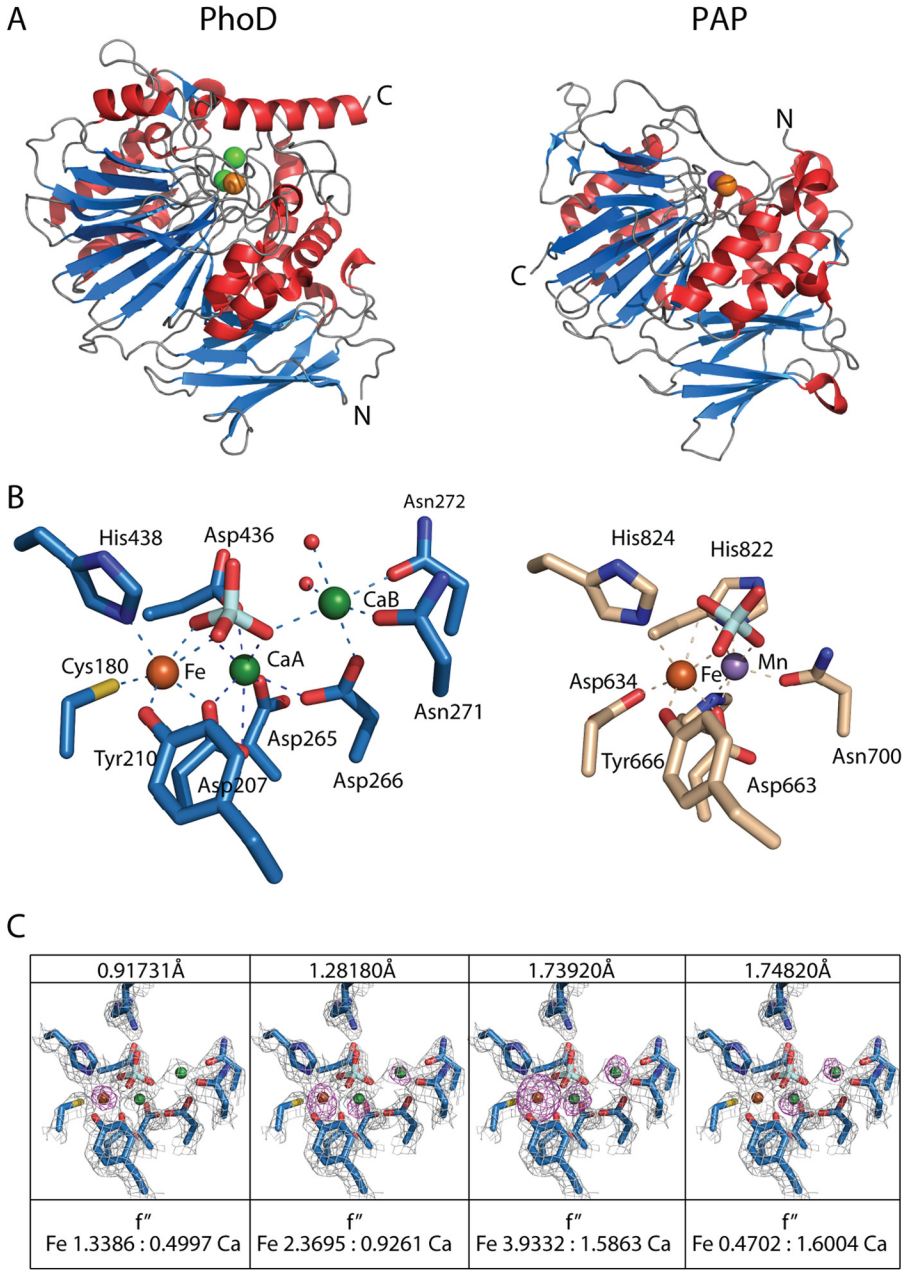

FIGURE 3. **PhoD has structural similarity to purple acid phosphatases.** *A*, comparison of the overall fold of PhoD (*left*) and sweet potato PAP (PDB 1XZW) (*right*). Both structures are shown in the same orientation with β-strands colored *blue* and α-helices colored *red*. The catalytic site metal ions are presented as *spheres*, with Fe^{3+} shown in *orange*, Ca^{2+} shown in *green*, and Mn^{2+} shown in purple. *B*, comparison of the coordination environment of the PhoD metal ions (*left*) with those in sweet potato PAP (*right*). Metal ions are colored as in *A*, and other atoms are colored as follows: oxygen in *red*; nitrogen in *dark blue*; sulfur in *yellow*; phosphorus in *light blue*; PhoD carbons in *sky blue*; and PAP carbons in *tan*. Metal ion coordination bonds are shown by *dashed lines*. Alignment between the proteins was carried out with LSQKAB (44). *C*, electron density at the PhoD active site contoured at 1σ (*gray*) overlaid with anomalous Fourier maps contoured at 4σ (*purple*) at the x-ray wavelengths indicated at the top of each panel. The anomalous signals for iron relative to calcium are consistent with the theoretical f″ values for iron and calcium at these wavelengths calculated using Crossec (45), which are given under the panels.

the main body of PhoD and could plausibly be released at some stage of the catalytic cycle. Attempts to observe the predicted movement of the C-terminal helix by co-crystallization with the bulky substrate analogues phosphonoacetic acid and phosphonohexanoic in place of phosphate were unsuccessful.

The function of the PhoD C-terminal helix was investigated using variants possessing truncations of this helix. These experiments show that the whole C-terminal helix is required for catalytic activity and that even the variant with the smallest truncation tested had lost the visible absorbance bands arising from the Fe^{3+} ion (Fig. 7). Thus the C-terminal helix is required to either insert or retain the PhoD active site metal cofactor.

DISCUSSION

The structure of *B. subtilis* PhoD confirms earlier suggestions (9) that PhoD family proteins have structural features in common with eukaryotic PAPs. The two protein families share the same protein fold, and both contain a tyrosinate-ligated Fe^{3+} ion at the same position in the active site. Indeed, the sole difference in the Fe^{3+} coordination environment between

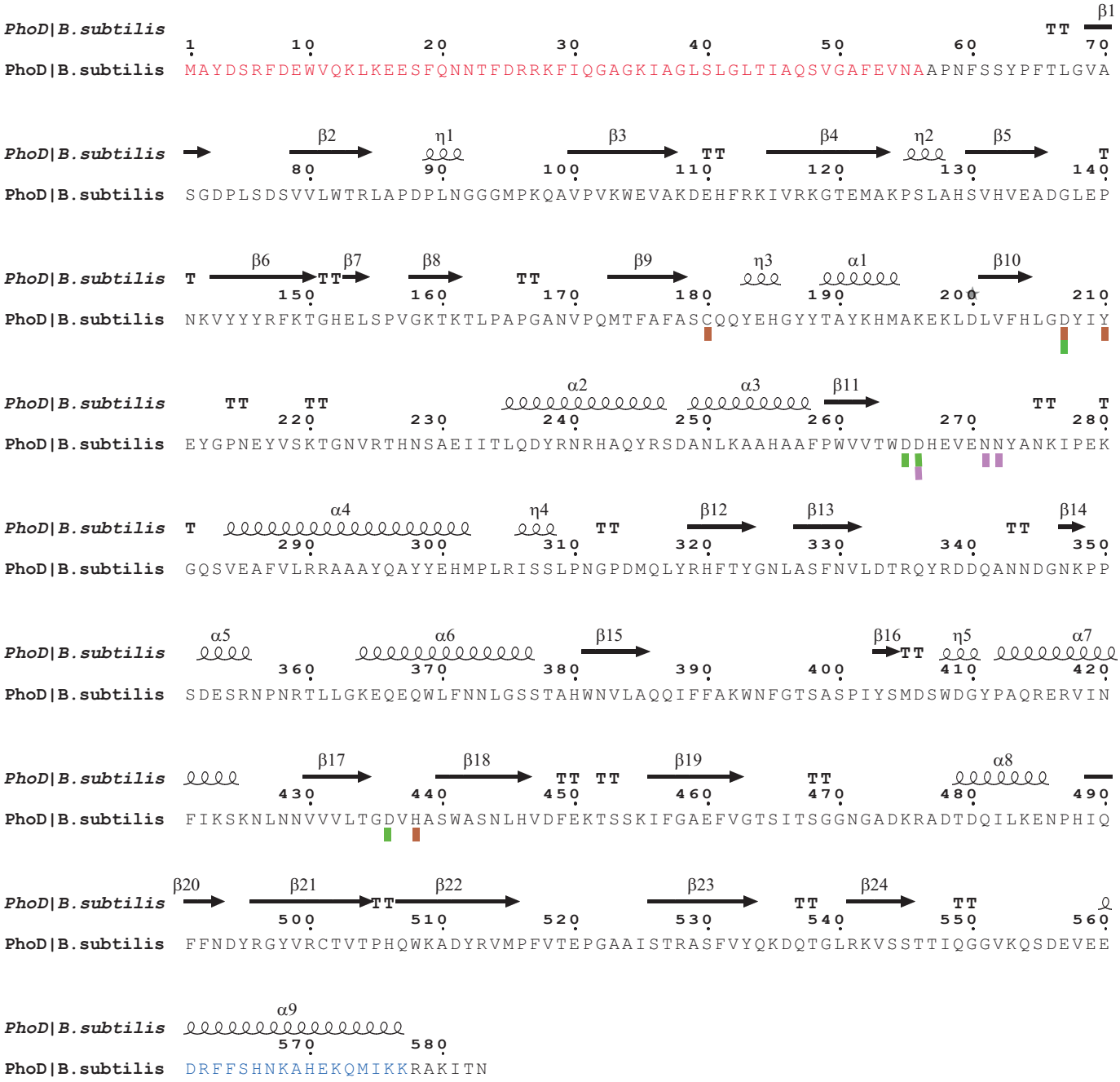

FIGURE 4. **Amino acid sequence of PhoD.** The secondary structure elements are shown above the sequence, with α-helices represented by *squiggles*, β strands represented by *arrows*, and turns represented by the letters *TT*. The signal peptide is highlighted in *red*, and the C-terminal α-helix is highlighted in *blue*. Metal ligating residues are indicated by *blocks* beneath the sequence, with those coordinating the Fe ion in *brown*, Ca_A in *green*, and Ca_B in *purple*. Residues that coordinate two metal ions are indicated by *blocks with two colors*.

PAPS and *B. subtilis* PhoD is the substitution of one of the aspartic acid residues in the canonical PAPs ligand set by a cysteine (Cys-180). In this context it is worth noting that PhoD family proteins can be divided on sequence grounds into two subfamilies, one of which possesses the cysteine Fe^{3+} ligand seen in *B. subtilis* PhoD and also *S. chromofuscus* PLD, whereas the second has the aspartate ligand found in the PAPS site.

Notwithstanding their similarities, the PhoD and PAPs families clearly form distinct sequence groups and differ in their active site metal complement beyond the tyrosine-ligated Fe^{3+} ion. Although the PAPs bind an additional Fe^{2+}, Mn^{2+}, or Zn^{2+} ion, *B. subtilis* PhoD binds two Ca^{2+} ions. Other members of the PhoD family almost certainly bind the same two Ca^{2+} ions because the coordinating amino acids are close to invariant within the family (the residue equivalent to *B. subtilis* PhoD Ca_B ligand Asn-272 is sometimes conservatively substituted with an Asp, which is also a good Ca^{2+} ligand). Although the position of the Ca_A ion in PhoD is similar to that of the divalent ion in the PAPs, the ligand sets provided by the two protein families are completely distinct. Ca_A in PhoD has five coordination bonds from Asp residues, whereas the divalent ion in PAPs is ligated by an invariant $His_2Asp_1Asn_1$ set (31). It

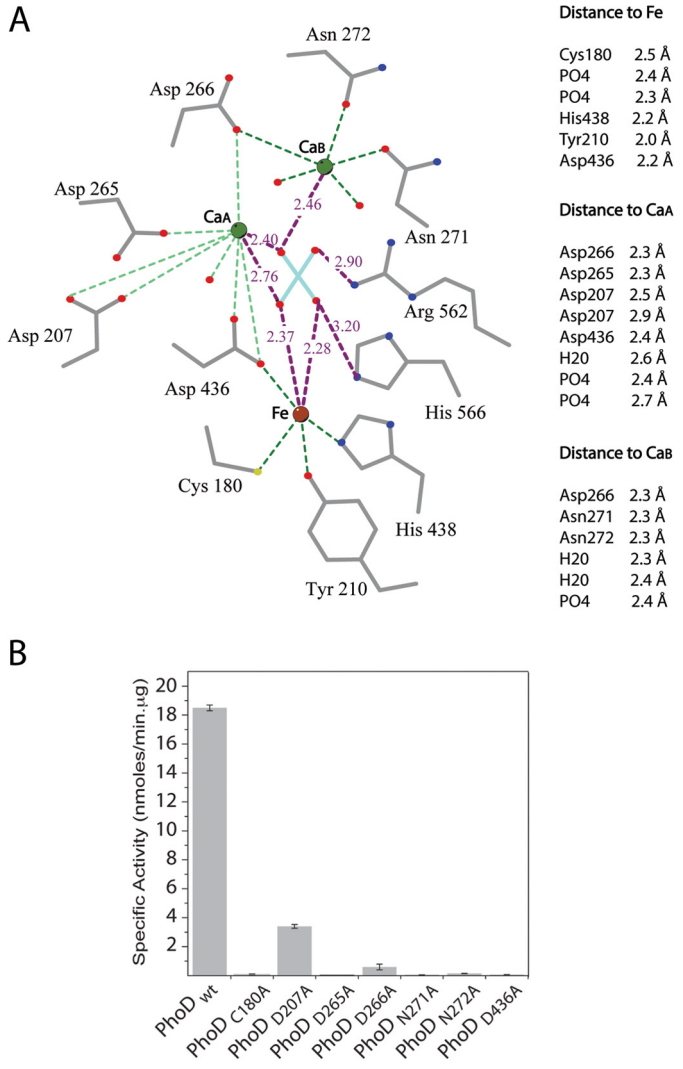

FIGURE 5. **Characterization of the PhoD active site.** *A*, diagrammatic representation of bonding interactions in the PhoD active site. Amino acid side chains and the bound phosphate ion are shown in sticks representation with carbon atoms in *gray*, oxygen atoms in *red*, nitrogen atoms in *blue*, phosphorus atom in *cyan*, and sulfur atom in *yellow*. Bonding interactions are represented by *dotted lines*. Bond distances in Å to the phosphate ion are marked on the figure. Other metal ion-ligand distances are tabulated at the *right-hand side* of the figure. The figure was drawn using LIGPLOT (46). *B*, phosphatase activity of PhoD active site variants using pNPP as substrate. PhoD wt is the wild-type protein. *Error bars* indicate the S.D. of three independent experiments.

should be noted that the earlier predictions for the non-iron ion ligands in the PhoD family are incorrect (9). A few bacteria encode proteins that conserve all PAP metal ligands (32), and these proteins can be considered to be true bacterial PAPs. By contrast, our structural analysis shows that the much more widely distributed enzymes of the PhoD family should be regarded as forming a distinct but closely related sister group to the PAPs. Because *B. subtilis* PhoD and *S. chromofuscus* PLD are thought to target specific phosphate-containing molecules *in vivo* (teichoic acids and phospholipids, respectively) it is possible that other PhoD family members also have specialist biological roles rather than operating as general phosphatases like members of the PhoA and PhoX families.

B. subtilis PhoD has a flexible C-terminal helix overlaying the active site (Fig. 7). Although this helix is not present in most other members of the PhoD family, analogous "cap domains" are a feature of certain other enzymes in the metallophosphatase superfamily (33–36). In most cases the role of these cap domains is unclear. Intriguingly, however, the cap domain of a mycobacterial metallophosphatase has recently been implicated in cell wall binding (33). An equivalent function for the PhoD C-terminal helix is an attractive hypothesis given the proposed role of PhoD in teichoic acid metabolism.

The way in which phosphate is bound to the active site of PhoD in our crystal structure is likely to mimic the substrate-enzyme interaction at some point in the catalytic reaction. We can get considerable insight into the likely mechanism of PhoD catalysis by interpreting the phosphate complex in the light of the extensive body of work on the mechanism of PAPs. In PAPs the two active site metal ions are bridged by a hydroxide ion. The current view is that phosphomonoester substrates coordinate both PAP metal ions. The bridging hydroxide ion then undertakes a nucleophilic attack on the phosphorus atom in-line with the bond to the leaving group. This results in the hydroxide ion being incorporated into the phosphate product (10). A structure has been determined for sweet potato PAP in which a phosphate ion is bound in a tripodal μ–η2–η2-geometry between the two metals ions such that one of the oxygen atoms occupies the position normally taken by the bridging hydroxide ion (26). This structure has been interpreted as representing the initial product complex in which the oxygen atom of the hydroxide nucleophile is fully bonded to the substrate phosphorus atom while still maintaining bridging coordination to the metal ions. The position of the phosphate ion in the PhoD structure is highly analogous to that in the sweet potato PAPs structure (Fig. 3*B*), suggesting that PhoD possesses a nucleophilic hydroxide between the Fe and Ca_A ions and that the PhoD structure represents the initial product complex formed by the reaction involving this ion.

PhoD is a phosphodiesterase and so must be capable of catalyzing two successive hydrolysis reactions. This process could involve repeating the reaction involving the bridging hydroxide, with the initial product rotating in the active site before the second reaction. Alternatively, the two reactions could utilize distinct nucleophiles. Comparisons with the PAPs are again potentially informative in distinguishing between these two possibilities. Although PAPs have historically been considered not to catalyze phosphodiesterase reactions due to their inability to hydrolyze bis-pNPP (37) recent work with less sterically restricted substrates has shown that PAPs do possess this capability (38). The inferred phosphodiesterase mechanism in the PAPs is nucleophilic attack by a Fe^{3+}-coordinated terminal hydroxide group followed by a second nucleophilic attack by the bridging hydroxide. A similar mechanism is plausible for PhoD with the phosphate complex corresponding to the initial product of the second hydrolytic reaction.

A striking difference between the PhoD and PAP families (and, indeed, other members of the metallophosphatase superfamily) is the presence of a third metal ion (Ca_B) in PhoD. Because PAPs are able to catalyze phosphodiesterase reactions at a similar rate to phosphomonoester hydrolysis with only two metal ions (38) it is unlikely that the presence of CaB is specifically linked to the phosphodiesterase functionality of PhoD.

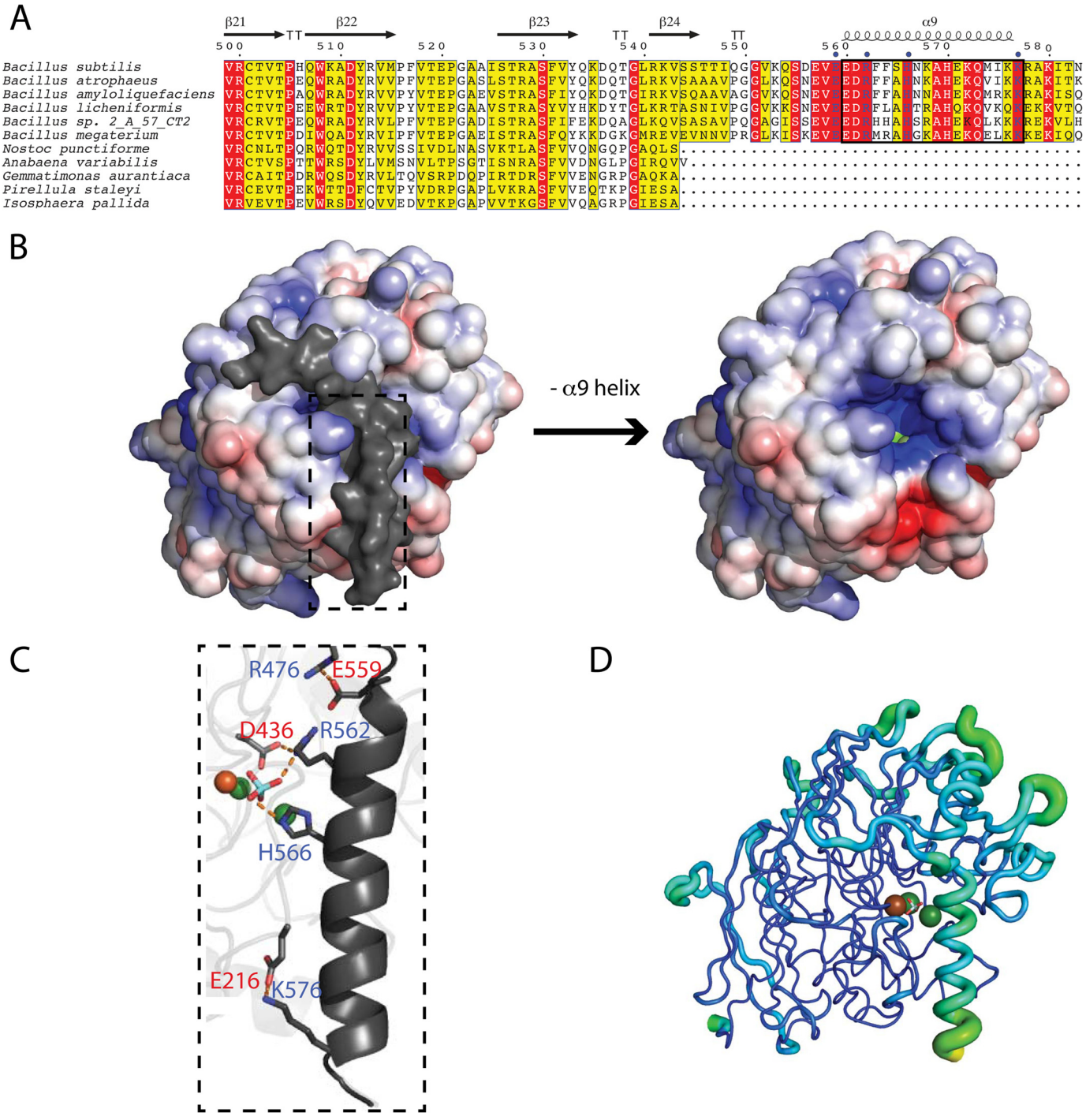

FIGURE 6. **The C-terminal helix of PhoD occludes the active site.** *A*, multiple sequence alignment of the C termini of PhoD family proteins showing the extension seen in the PhoD protein of *B. subtilis* and some other *Bacillus* species. Secondary structure elements from the *B. subtilis* PhoD structure are shown above the alignment with the α-helix shown as a *coil*, β-strands shown as *arrows*, and β-turns shown by the *letter T*. Conserved amino acids are highlighted in *red*, and similar amino acids are highlighted in *yellow*. The *black box* indicates the C-terminal α-helix of *B. subtilis* PhoD. Residues in the C terminus involved in salt bridges with the main structure (colored *blue*) are indicated with *blue dots* above the alignment. *B*, electrostatic surface model (± 5 *kT*/*e*) of intact PhoD (*left*) and with the C-terminal helix removed (*right*). Regions of negative charge are shown in *red*, and regions of positive charge are shown in *blue*, but with the C-terminal helix in *gray*. Electrostatic calculations were performed with APBS (47) and include the charges on the active site metal ions. *C*, the salt bridge network between the C-terminal helix, the bound phosphate ion, and the active site. The portion of PhoD shown corresponds to the region of the PhoD structure highlighted in *panel B*. *D*, B-factor putty diagram of PhoD generated by PyMOL. Flexibility is indicated by increasing ribbon girth and color scaling from *blue* to *green*.

Instead, Ca_B is appropriately placed to stabilize the developing charge on the leaving group during nucleophilic attack by the bridging hydroxide ion. More generally, the additional metal ion may compensate for the weaker polarizing ability of Ca^{2+} relative to the divalent metal ions found in the PAPs (Fe^{2+}, Mn^{2+}, Zn^{2+}).

The combination of Fe^{3+} and Ca^{2+} ions used by PhoD is unusual and to the best of our knowledge has only otherwise

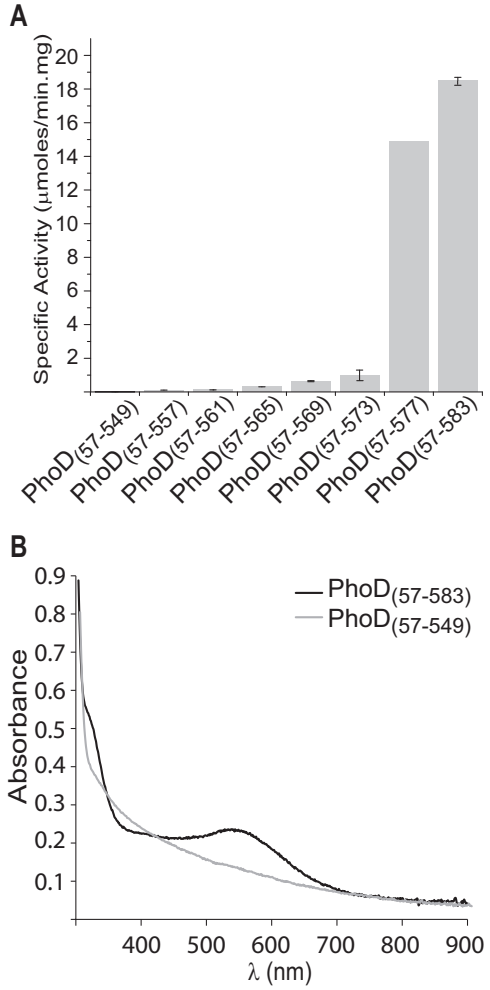

FIGURE 7. **The C-terminal helix of PhoD is functionally important.** *A*, phosphatase activity of C-terminally truncated PhoD variants. PhoD (57–583) is the intact protein. Activities were measured using pNPP as substrate. *Error bars* indicate the S.D. of three independent experiments. *B*, visible absorption spectra of wild-type PhoD (57–583)(*black line*) and the C-terminal truncation variant (57–549)(*gray line*).

been seen in the structurally unrelated PhoX alkaline phosphatase (4). Remarkably, therefore, two out of the three major classes of alkaline phosphatases in bacteria use the same, rare combination of metal ions. Both PhoD and PhoX are extracytoplasmic bacterial enzymes, and so the selection of Ca^{2+} as the divalent cation may simply reflect the high availability of Ca^{2+} ions in most terrestrial and marine environments (39). By contrast, the bioavailability of iron is low in many environments (40) and may limit the activity of PhoD family enzymes in such locations, as has also recently been argued for PhoX (4). Export of both PhoD and PhoX family proteins uses the Tat protein translocation system, which is dedicated to the transport of folded proteins (41–43). The Tat pathway is often used by proteins that need to fold before export to bind cofactor molecules in the cytoplasm. We speculate that the limited availability of soluble iron in the external environment means that biosynthesis of PhoD and PhoX cannot rely on the acquisition of adventitious iron in the periplasm. Iron ions would, instead, be inserted into these proteins under controlled conditions in the cytoplasm with export of the folded, iron-containing, proteins taking place via the Tat apparatus. In summary, the PhoD structure reveals that members of this widely distributed family of bacterial enzymes represent a new class of Fe^{3+}- and Ca^{2+}-dependent phosphatase.

Acknowledgments—We thank Oliver Zeldin and Elspeth Garman for micro-PIXE measurements, Janet Lovett for assistance with the EPR measurements, Jeff Errington for providing B. subtilis 168 genomic DNA, and Shee Chien Yong, Magda Atilano, Petros Ligoxygakis, and Richard Daniel for discussions. We also thank the staff of beamline ID23_1 of the European Synchrotron Radiation Facility, Grenoble, France. We acknowledge the Diamond Light Source for time on beamline I03 under proposal MX9306.

REFERENCES

1. Rusch, D. B., Halpern, A. L., Sutton, G., Heidelberg, K. B., Williamson, S., Yooseph, S., Wu, D., Eisen, J. A., Hoffman, J. M., Remington, K., Beeson, K., Tran, B., Smith, H., Baden-Tillson, H., Stewart, C., Thorpe, J., Freeman, J., Andrews-Pfannkoch, C., Venter, J. E., Li, K., Kravitz, S., Heidelberg, J. F., Utterback, T., Rogers, Y. H., Falcón, L. I., Souza, V., Bonilla-Rosso, G., Eguiarte, L. E., Karl, D. M., Sathyendranath, S., Platt, T., Bermingham, E., Gallardo, V., Tamayo-Castillo, G., Ferrari, M. R., Strausberg, R. L., Nealson, K., Friedman, R., Frazier, M., and Venter, J. C. (2007) The Sorcerer II Global Ocean Sampling expedition: northwest Atlantic through eastern tropical Pacific. *PLoS Biol.* **5,** e77
2. Luo, H., Benner, R., Long, R. A., and Hu, J. (2009) Subcellular localization of marine bacterial alkaline phosphatases. *Proc. Natl. Acad. Sci. U.S.A.* **106,** 21219–21223
3. Lassila, J. K., Zalatan, J. G., and Herschlag, D. (2011) Biological phosphoryl-transfer reactions: understanding mechanism and catalysis. *Annu. Rev. Biochem.* **80,** 669–702
4. Yong, S.C., Roversi, P., Lillington, J., Rodriguez, F., Krehenbrink, M., Zeldin, O. B., Garman, E. F., Lea, S. M., and Berks, B. C. (2014) A complex iron-calcium cofactor catalyzing phosphotransfer chemistry. *Science* **345,** 1170–1173
5. Yamane, K., and Maruo, B. (1978) Purification and characterization of extracellular soluble and membrane-bound insoluble alkaline phosphatases possessing phosphodiesterase activities in *Bacillus subtilis*. *J. Bacteriol.* **134,** 100–107
6. Eder, S., Shi, L., Jensen, K., Yamane, K., and Hulett, F. M. (1996) A *Bacillus subtilis* secreted phosphodiesterase/alkaline phosphatase is the product of a Pho regulon gene, *phoD*. *Microbiology* **142,** 2041–2047
7. Zambonelli, C., and Roberts, M. F. (2003) An iron-dependent bacterial phospholipase D reminiscent of purple acid phosphatases. *J. Biol. Chem.* **278,** 13706–13711
8. Marchler-Bauer, A., Zheng, C., Chitsaz, F., Derbyshire, M. K., Geer, L. Y., Geer, R. C., Gonzales, N. R., Gwadz, M., Hurwitz, D. I., Lanczycki, C. J., Lu, F., Lu, S., Marchler, G. H., Song, J. S., Thanki, N., Yamashita, R. A., Zhang, D., and Bryant, S. H. (2013) CDD: conserved domains and protein three-dimensional structure. *Nucleic Acids Res.* **41,** D348–D352
9. Zambonelli, C., Casali, M., and Roberts, M. F. (2003) Mutagenesis of putative catalytic and regulatory residues of *Streptomyces chromofuscus* phospholipase D differentially modifies phosphatase and phosphodiesterase activities. *J. Biol. Chem.* **278,** 52282–52289
10. Schenk, G., Mitić, N., Gahan, L. R., Ollis, D. L., McGeary, R. P., and Guddat, L. W. (2012) Binuclear metallohydrolases: complex mechanistic strategies for a simple chemical reaction. *Acc. Chem. Res.* **45,** 1593–1603
11. Mitić, N., Smith, S. J., Neves, A., Guddat, L. W., Gahan, L. R., and Schenk, G. (2006) The catalytic mechanisms of binuclear metallohydrolases. *Chem. Rev.* **106,** 3338–3363
12. Ferrer, M., Golyshina, O. V., Beloqui, A., Bottger, L. H., Andreu, J. M., Polaina, J., De Lacey, A. L., Trautwein, A. X., Timmis, K. N., and Golyshin, P. N. (2008) A purple acidophilic di-ferric DNA ligase from *Ferroplasma*. *Proc. Natl. Acad. Sci. U.S.A.* **105,** 8878–8883
13. Andréasson, C., Fiaux, J., Rampelt, H., Mayer, M. P., and Bukau, B. (2008)

Hsp110 is a nucleotide-activated exchange factor for Hsp70. *J. Biol. Chem.* **283,** 8877–8884
14. Studier, F. W., Rosenberg, A. H., Dunn, J. J., and Dubendorff, J. W. (1990) Use of T7 RNA polymerase to direct expression of cloned genes. *Methods Enzymol.* **185,** 60–89
15. Vonrhein, C., Flensburg, C., Keller, P., Sharff, A., Smart, O., Paciorek, W., Womack, T., and Bricogne, G. (2011) Data processing and analysis with the autoPROC toolbox. *Acta Crystallogr. D Biol. Crystallogr.* **67,** 293–302
16. Bricogne, G., Vonrhein, C., Flensburg, C., Schiltz, M., and Paciorek, W. (2003) Generation, representation and flow of phase information in structure determination: recent developments in and around SHARP 2.0. *Acta Crystallogr. D Biol. Crystallogr.* **59,** 2023–2030
17. Abrahams, J. P., and Leslie, A. G. W. (1996) Methods used in the structure determination of bovine mitochondrial F_1 ATPase. *Acta Crystallogr. D Biol. Crystallogr.* **52,** 30–42
18. Cowtan, K. (2006) The Buccaneer software for automated model building. 1. Tracing protein chains. *Acta Crystallogr. D Biol. Crystallogr.* **62,** 1002–1011
19. Vagin, A., and Teplyakov, A. (1997) MOLREP: an automated program for molecular replacament. *J. Appl. Crystallogr.* **30,** 1022–1025
20. Murshudov, G. N., Vagin, A. A., and Dodson, E. J. (1997) Refinement of macromolecular structures by the maximum-likelihood method. *Acta Crystallogr. D Biol. Crystallogr.* **53,** 240–255
21. Emsley, P., and Cowtan, K. (2004) Coot: model-building tools for molecular graphics. *Acta Crystallogr. D Biol. Crystallogr.* **60,** 2126–2132
22. Davis, I. W., Leaver-Fay, A., Chen, V. B., Block, J. N., Kapral, G. J., Wang, X., Murray, L. W., Arendall, W. B., 3rd, Snoeyink, J., Richardson, J. S., and Richardson, D. C. (2007) MolProbity: all-atom contacts and structure validation for proteins and nucleic acids. *Nucleic Acids Res.* **35,** W375–W383
23. Stoll, S., and Schweiger, A. (2006) EasySpin, a comprehensive software package for spectral simulation and analysis in EPR. *J. Magn. Reson.* **178,** 42–55
24. Holm, L., and Rosenström, P. (2010) Dali server: conservation mapping in 3D. *Nucleic Acids Res.* **38,** W545–W549
25. Feder, D., Hussein, W. M., Clayton, D. J., Kan, M. W., Schenk, G., McGeary, R. P., and Guddat, L. W. (2012) Identification of purple acid phosphatase inhibitors by fragment-based screening: promising new leads for osteoporosis therapeutics. *Chem. Biol. Drug Des.* **80,** 665–674
26. Schenk, G., Gahan, L. R., Carrington, L. E., Mitic, N., Valizadeh, M., Hamilton, S. E., de Jersey, J., and Guddat, L. W. (2005) Phosphate forms an unusual tripodal complex with the Fe-Mn center of sweet potato purple acid phosphatase. *Proc. Natl. Acad. Sci. U.S.A.* **102,** 273–278
27. Gaber, B. P., Sheridan, J. P., Bazer, F. W., and Roberts, R. M. (1979) Resonance Raman scattering from uteroferrin, the purple glycoprotein of the porcine uterus. *J. Biol. Chem.* **254,** 8340–8342
28. Oganesyan, V. S., and Thomson, A. J. (2000) Magnetic circular dichroism of symmetry and spin forbidden transitions of high-spin metal ions. *J. Chem. Phys.* **113,** 5003–5017
29. Benini, S., Rypniewski, W. R., Wilson, K. S., Ciurli, S., and Mangani, S. (2001) Structure-based rationalization of urease inhibition by phosphate: novel insights into the enzyme mechanism. *J. Biol. Inorg. Chem.* **6,** 778–790
30. Ely, F., Pedroso, M. M., Gahan, L. R., Ollis, D. L., Guddat, L. W., and Schenk, G. (2012) Phosphate-bound structure of an organophosphate-degrading enzyme from *Agrobacterium radiobacter*. *J. Inorg. Biochem.* **106,** 19–22
31. Guddat, L. W., McAlpine, A. S., Hume, D., Hamilton, S., de Jersey, J., and Martin, J. L. (1999) Crystal structure of mammalian purple acid phosphatase. *Structure* **7,** 757–767
32. Schenk, G., Korsinczky, M. L., Hume, D. A., Hamilton, S., and DeJersey, J. (2000) Purple acid phosphatases from bacteria: similarities to mammalian and plant enzymes. *Gene* **255,** 419–424
33. Matange, N., Podobnik, M., and Visweswariah, S. S. (2014) The non-catalytic "cap domain" of a mycobacterial metallophosphoesterase regulates its expression and localization in the cell. *J. Biol. Chem.* **289,** 22470–22481
34. Miller, D. J., Shuvalova, L., Evdokimova, E., Savchenko, A., Yakunin, A. F., and Anderson, W. F. (2007) Structural and biochemical characterization of a novel Mn^{2+}-dependent phosphodiesterase encoded by the *yfcE* gene. *Protein Sci.* **16,** 1338–1348
35. Jackson, C. J., Carr, P. D., Liu, J. W., Watt, S. J., Beck, J. L., and Ollis, D. L. (2007) The structure and function of a novel glycerophosphodiesterase from *Enterobacter aerogenes*. *J. Mol. Biol.* **367,** 1047–1062
36. Dermol, U., Janardan, V., Tyagi, R., Visweswariah, S. S., and Podobnik, M. (2011) Unique utilization of a phosphoprotein phosphatase fold by a mammalian phosphodiesterase associated with WAGR syndrome. *J. Mol. Biol.* **412,** 481–494
37. Schlosnagle, D. C., Bazer, F. W., Tsibris, J. C., and Roberts, R. M. (1974) An iron-containing phosphatase induced by progesterone in the uterine fluids of pigs. *J. Biol. Chem.* **249,** 7574–7579
38. Cox, R. S., Schenk, G., Mitić, N., Gahan, L. R., and Hengge, A. C. (2007) Diesterase activity and substrate binding in purple acid phosphatases. *J. Am. Chem. Soc.* **129,** 9550–9551
39. Fraústo da Silva, J. J. R., and Williams, R. J. P. (2001) *The Biological Chemistry of the Elements: The Inorganic Chemistry of Life*, 2nd Ed., Oxford University Press, Oxford
40. Moore, C. M., Mills, M. M., Arrigo, K. R., Berman-Frank, I., Bopp, L., Boyd, P. W., Galbraith, E. D., Geider, R. J., Guieu, C., Jaccard, S. L., Jickells, T. D., La Roche, J., Lenton, T. M., Mahowald, N. M., Maranon, E., Marinov, I., Moore, J. K., Nakatsuka, T., Oschlies, A., Saito, M. A., Thingstad, T. F., Tsuda, A., and Ulloa, O. (2013) Processes and patterns of oceanic nutrient limitation. *Nat. Geosci.* **6,** 701–710
41. Palmer, T., and Berks, B. C. (2012) The twin-arginine translocation (Tat) protein export pathway. *Nat. Rev. Microbiol.* **10,** 483–496
42. Jongbloed, J. D., Martin, U., Antelmann, H., Hecker, M., Tjalsma, H., Venema, G., Bron, S., van Dijl, J. M., and Müller, J. (2000) TatC is a specificity determinant for protein secretion via the twin-arginine translocation pathway. *J. Biol. Chem.* **275,** 41350–41357
43. Yang, H., and Roberts, M. F. (2004) Expression and characterization of a heterodimer of *Streptomyces chromofuscus* phospholipase D. *Biochim. Biophys. Acta* **1703,** 43–51
44. Kabsch, W. (1976) A solution for the best rotation to relate two sets of vectors. *Acta Crystallogr. A* **32,** 922–923
45. Cromer, D. T. (1983) Calculation of anomalous scattering factors at arbitrary wavelengths. *J Appl. Crystallogr.* **16,** 437–438
46. Wallace, A. C., Laskowski, R. A., and Thornton, J. M. (1995) Ligplot: a program to generate schematic diagrams of protein ligand interactions. *Protein Eng.* **8,** 127–134
47. Baker, N. A., Sept, D., Joseph, S., Holst, M. J., and McCammon, J. A. (2001) Electrostatics of nanosystems: Application to microtubules and the ribosome. *Proc. Natl. Acad. Sci. U.S.A.* **98,** 10037–10041